Dalton Transactions

RSC Publishing

PAPER

View Article Online
View Journal | View Issue

Defective dicubanes of Co^{II}/Co^{III} complexes with triethanolamine and N-donors†

Cite this: *Dalton Trans.*, 2013, **42**, 5355

S. R. Hosseinian,[a] V. Tangoulis,*[a] M. Menelaou,[a] C. P. Raptopoulou,[b] V. Psycharis[b] and C. Dendrinou-Samara*[a]

The mixed valence Co^{II}/Co^{III} tetranuclear clusters $[Co^{II}_2Co^{III}_2(tea)_2(pyr)_2(NO_3)_4]\cdot 2CH_3CN$ (**1**), $[Co^{II}_2Co^{III}_2(\mu_3\text{-}OH)_2(Htea)_2(bpy)_4](NO_3)_4$ (**2**), and $[Co^{II}_2Co^{III}_2(\mu_3\text{-}OH)_2(Htea)_2(phen)_4](NO_3)_4\cdot 2CH_3CN\cdot 2CH_3OH$ (**3**) are described where tea and Htea are the fully and the doubly deprotonated form of triethanolamine, while as N-donors are pyridine, 2,2′-bipyridine and 1,10-phenanthroline. Complexes **1–3** contain the $Co^{II}_2Co^{III}_2O_6$ core and can be described as defective dicubanes with different imperfectness. In **1**, the central rhombic core Co_2O_2 is occupied by two Co^{III} ions while the external cobalt atoms display Co^{II} oxidation states; meanwhile **2** and **3** exhibit a reversal in their $Co^{II}_2Co^{III}_2$ oxidation state distribution. Two different theoretical models were used to explain the magnetic behavior: (i) spin–spin interaction model with local anisotropy terms where $S = 3/2$ for both metal centers and (ii) an anisotropic spin–spin interaction model applicable in the low temperature range ($T < 40$ K) using effective spins ($S_{eff} = 1/2$) for both metal centers. For **1** a relatively strong next-nearest-neighbour antiferromagnetic exchange interaction between the Co(II) centers which are connected *via* diamagnetic Co(III) ion was found while for **2** and **3** the presence of ferromagnetic interaction is confirmed. The fitting results, concerning the first model, gave: $J = 2.0(2)/3.2(2)/3.8(2)$ cm^{-1}, $g = 2.35(1)/2.52(1)/2.57(1)$ and $D = 11.0(1)/8.5(1)/7.8(1)$ cm^{-1} while concerning the second model are: $J_z = -7.1(2)/19.2(2)/22.1(2)$ cm^{-1}, $g_z = 6.8(1)/8.1(1)/8.3(1)$, $J_{xy}/J_z = 0.34(2)/0.11(2)/0.14(2)$, and $g_{xy}/g_z = 0.52(2)/0.28(2)/0.36(2)$ for **1–3**. X-Band EPR spectrum of **1** has a very broad derivative centered at $g = 5.3$ while for **2** and **3** large g-variations were found in the range 20.0–1.0, indicative of an exchange interaction between Co(II) ions.

Received 1st November 2012,
Accepted 21st December 2012

DOI: 10.1039/c2dt32616g

www.rsc.org/dalton

Introduction

Tetranuclearity can be considered a common and representative class of high-nuclearity 3d-metal clusters showing interesting properties spanning from catalysis,[1] and magnetism[2] to modelling biochemical reactions.[3] Various coordination motifs have been described in the literature in which the M_4 cores present linear,[4] cubane,[5] butterfly,[6] adamantane,[7] basket,[8] squares,[9] and metallacrown[10] topologies. Cubane-like clusters, found in a variety of transition metal complexes, exhibit interesting magnetic exchange properties and under certain circumstances act as single molecule magnets.[11] In biology, such systems are well known;[12] the Fe_4S_4 cubane units are present in the structure of a ferredoxin protein[13] and act as electron transfer agents,[14] the heteronuclear cubane Mn_3CaO_4 is present at the active site of the oxygen evolving centre of photosystem II,[15] and the Fe_3MoS_4 has been identified at the active site of nitrogenase.[16]

Cubane-like structures favored in iron,[17] manganese[18] and vanadium[19] hydroxo- and/or alkoxo-bridged chemistry, while in cobalt systems are relatively limited especially the mixed valence Co^{II}/Co^{III} compounds. Although we have little synthetic control to form such complexes, as most of them are obtained serendipitously, one of the most fruitful routes can be considered to be the use of multidentate binding ligands along with bridging anions such as N_3^-,[20] CH_3O^-,[21] *etc.* To our knowledge till now, the reported tetranuclear mixed valence Co^{II}/Co^{III} clusters showing cubane-like structures have been isolated in the presence of: (a) aminoalcohol ligands; $[Co_2Co_2(H_2hbhpd)_2(H_4hbhpd)_2(H_2O)_2]\cdot Cl_2\cdot (CH_3OH)_4$,[22] (where H_5hbhpd = 2-(2-hydroxy-benzylamino)-2-hydroxymethyl-propane-1,3-diol), $[Co_2Co_2\{NH(C_2H_4OH)_2\}_2\{NH(C_2H_4O)_2\}_4](ClO_4)$,[23] (b) multidentate Schiff base ligands; $[Co_2Co_2L_2(CH_3O)_4]\cdot 2CH_2Cl_2$[24] (where H_3L = bis(benzoylacetone)-1,3-diiminopropan-2-ol), $[Co_2Co_2(C_{14}H_{19}O_3N_2)_2(\mu_3\text{-}OMe)_2$-

[a]*Department of General and Inorganic Chemistry, School of Chemistry, Aristotle University of Thessaloniki, Thessaloniki, 54124, Greece. E-mail: samkat@chem.auth.gr; Fax: +30 2310997738; Tel: +30 2310997876*
[b]*NCSR "Demokritos", Institute of Advanced Materials, Physicochemical Processes, Nanotechnology and Microsystems, Department of Materials Science, 15310 Aghia Paraskevi Attikis, Greece*

†CCDC 905823 for **1**, 905824 for **2**, and 905825 for **3**. For crystallographic data in CIF or other electronic format see DOI: 10.1039/c2dt32616g

$(NO_3)(H_2O)_2](NO_3)\cdot 2(H_2O)$,[25] $[Co_2Co_2(\mu_{1,1}\text{-}N_3)_4(N_3)_2(HDMSP)_2(MeOH)_2]\cdot 2H_2O$,[26] (where H_3DMSP = 1,3-dihydroxy-2-methyl-2-(salicylideneamino)propane), $[Co_2Co_2(HL)_2(OCH_3)_2(N_3)_4]\cdot CH_3OH\cdot 2H_2O$,[27] $[Co_2Co_2(HL)_2(OCH_3)_2(N_3)_2(CH_3CO_2)_2]\cdot 2CH_3OH\cdot 2H_2O$,[27] $[Co_2Co_2(HL)_2(OCH_3)_2(CH_3OH)_2(N_3)_2](NO_3)_2$,[27] (where H_3L = 2,6-bis[(2-hydroxy-ethylimino)-methyl]-4-methylphenol), and (c) a diketone ligand; $[Co_2Co_2(C_5H_7O_2)_4(CH_3O)_4(C_2H_3O_2)_2]$.[28]

In view of the above and due to our ongoing interest for new preparative routes to polynuclear complexes of various transition metal complexes, we chose to investigate the coordination chemistry of cobalt in the presence of triethanolamine and neutral co-ligands, namely N-donors of different sizes. Triethanolamine (H_3tea) is an aminoalcohol that acts as a binder since it possesses four binding sites capable of coordinating metal ions with important features. Several structures are reported in the literature where triethanolamine participates in high-nuclearity clusters with a variety of lattice dimensionality, unique architecture and aesthetically pleasing structures indicating its use as a versatile and multidentate capable ligand.[29–31]

Herein, we present the synthesis, isolation and characterization of three new tetranuclear mixed valence Co^{II}/Co^{III} structures: $[Co^{II}_2Co^{III}_2(tea)_2(pyr)_2(NO_3)_4]\cdot 2CH_3CN$ (**1**), $[Co^{II}_2Co^{III}_2(\mu_3\text{-}OH)_2(Htea)_2(bpy)_4](NO_3)_4$ (**2**), and $[Co^{II}_2Co^{III}_2(\mu_3\text{-}OH)_2(Htea)_2(phen)_4](NO_3)_4\cdot 2CH_3CN\cdot 2CH_3OH$ (**3**) where tea and Htea are the fully and the doubly deprotonated form of triethanolamine, while as co-ligands are the N-donor pyridine (= pyr), 2,2′-bipyridine (= bpy) and 1,10-phenanthroline (= phen) respectively. The variable-temperature magnetic susceptibilities of complexes **1–3** have been measured in the range 2–300 K under various external fields in the range 0.02–1.0 T. X-Band EPR spectra of **1–3** were recorded at 4–70 K. The magnetic behavior of the tetranuclear compounds **1–3** have been explained with two different theoretical models: (i) spin–spin interaction model with local anisotropy terms where S = 3/2 for both metal centers and (ii) an anisotropic spin–spin interaction model applicable in the low temperature range (T < 40 K) using effective spins (S_{eff} = 1/2) for both metal centers.

Results and discussion

In an effort to delve into the coordination chemistry of cobalt in the presence of triethanolamine and N-donors, different synthetic approaches were used. During these synthetic attempts and in a solvent mixture comprising MeCN–MeOH (1 : 1 v/v), the equimolar $Co(NO_3)_2$/H_3tea/Pyr reaction system in basic conditions monitoring with the relatively weak base triethylamine (Et_3N), resulted **1** in low yield (≥20%) as well as two other clusters; a pentanuclear and a heptanuclear one which are discussed elsewhere.[32] However, keeping all the reaction conditions as described above and by varying only the N-donor to 2,2′-bipyridine or 1,10-phenanthroline, **2** and **3** complexes were formed, respectively as the only products from each system in high yield (≥60%). Alternatively, complex **1** has been successfully prepared in high yield (≥70%) in pure MeCN. The purity of **1–3** was confirmed by powder X-ray diffraction and in comparison with their single crystal analysis.

The formation of **1–3** can be represented by the following equations (eqn (1)–(3)):

$$4Co(NO_3)_2 + 2H_3tea + 2pyr + 4Et_3N + 0.5O_2 + H_2O \rightarrow 4Et_3NH^+ + [Co^{II}_2Co^{III}_2(tea)_2(pyr)_2(NO_3)_4] + 4(NO_3)^- + 2H_2O \quad (1)$$

$$4Co(NO_3)_2 + 2H_3tea + 4bpy + 4Et_3N + 0.5O_2 + H_2O \rightarrow 4Et_3NH^+ + [Co^{II}_2Co^{III}_2(\mu_3\text{-}OH)_2(Htea)_2(bpy)_4]\cdot(NO_3)_4 + 4(NO_3)^- \quad (2)$$

$$4Co(NO_3)_2 + 2H_3tea + 4phen + 4Et_3N + 0.5O_2 + H_2O \rightarrow 4Et_3NH^+ + [Co^{II}_2Co^{III}_2(\mu_3\text{-}OH)_2(Htea)_2(phen)_4]\cdot(NO_3)_4 + 4(NO_3)^- \quad (3)$$

The oxidation of Co(II) to Co(III) ions is due to the presence of atmospheric O_2 and a process which has long been recognized in 3d-cluster chemistry (*e.g.* in manganese, iron and cobalt systems).[33] Moreover, triethylamine acts as a proton acceptor and thus facilitates the deprotonation of H_3tea and H_2O molecules resulted the HO^- groups found in **2** and **3**, respectively.[34] The incorporation of the nitrate anions can be considered crucial for the isolation of **1–3** acting either as a binding moiety as in **1** or providing the necessary charge for the crystallization in the case of **2** and **3**, respectively. Additionally, considering that the only difference between the reported complexes is the size of the N-donor, it seems that steric effects influence the formation of **2** and **3** while the formation of HO^- propagated only in the case of the N,N-donors. Therefore, the properties of the employed ligands in each ternary system are found to control the nuclearity but also the overall geometry of the resulting tetranuclear clusters with distinct coordination modes.[35]

The IR spectra of **1–3** exhibit characteristic vibrations of the C=N of the N-donor groups detected at 1607 cm^{-1} for **1**, 1610 cm^{-1} for **2** and 1625 cm^{-1} for **3** which correspond to the coordinated stretching frequencies of pyr, bpy and phen, respectively. Triethanolamine molecules have been assigned at three regions: (a) medium bands at 3400 cm^{-1} for **2** and **3** are assigned to the stretching vibrations of OH groups; (b) at about 2960 cm^{-1} and around 2930 cm^{-1} the ν_{as}(C–H) and ν_{sym}(C–H) are detected in **1–3**, respectively; and (c) three bands in the region of 1050 cm^{-1} are attributed to the ν(C–O) stretching in **1–3**. Additionally, in **2** and **3**, a strong band at 1384 cm^{-1} is assigned to the ionic nitrates.[36] The presence of the coordinated nitrates in **1** is indicative by two bands; the asymmetric stretching vibration of nitrate ν_{as}(–ONO_2) at 1479 cm^{-1} and the symmetric stretching vibration ν_{sym}(–ONO_2) at 1299 cm^{-1}. These vibrations do not occur in the ionic nitrates and the frequency difference $\Delta(\nu_{as} - \nu_{sym})$ found 180 cm^{-1} is correlated with the bidentate coordination mode

of the nitrate ions and is in good agreement with those found before.[37]

Description of the structures

General description. The single crystal X-ray determination of **1–3** revealed that in addition to lattice molecules and/or counter anions (CH_3CN for **1**, NO_3 for **2**, NO_3, CH_3OH and CH_3CN for **3**) they consist of tetranuclear centrosymmetric mixed valence Co^{II}/Co^{III} entities (neutral or cations) which can be best described as defective dicubanes with different imperfectness (Fig. 1–3). Complexes **2** and **3** can be considered analogous differing only in the size of N,N-donor co-ligand. The three clusters contain the $Co^{II}_2Co^{III}_2O_6$ core, meanwhile **1** exhibits a reversal in their $Co^{II}_2Co^{III}_2$ oxidation state distribution. All complexes possess a centre of symmetry which is located at the mid-point of the central rhombic core $\{Co_2O_2\}$. The two extreme corners are occupied by two Co(III) ions for **1** while in **2** and **3** by two Co(II) ions. In that respect, the core consists of four cobalt ions located at the three corners of two cubanes sharing in one face while in **2** and **3** complexes one vertex is missing and in complex **1** two vertexes are missing. Thus, they can be considered as defective dicubane cores divacant and tetravacant, respectively. Central oxygen atoms are provided by hydroxide ligands in **2** and **3** while in **1** are alkoxide oxygens coming from triethanolamine. Fig. 4 illustrates the core similarities of **1–3**.

Defective dicubane structure topology similar to **2** and **3** is common in $Mn^{II/III}$ chemistry[38] but rarely reported in $Co^{II/III}$ chemistry, meanwhile to our knowledge, the specific coordination pattern of **1** is reported for the first time.

Structure analysis of $[Co^{II}_2Co^{III}_2(tea)_2(pyr)_2(NO_3)_4]\cdot 2CH_3CN$ (1)

DIAMOND diagram of **1** appears in Fig. 1, while selected bond distances and angles are listed in Table 2. The tetranuclear cobalt complex in **1** is neutral and all cobalt ions exhibit distorted octahedral geometry. The fully deprotonated triethanolamine acts as 4.2221 ligand (Harris notation);[39] each alkoxide oxygen atom O(1), O(2) and O(3) is bridging the central cobalt ions Co(1), and from both sides the external cobalt ions Co(2) respectively while nitrogen (N(1)) from tea as well as nitrogen from pyridine molecule (N(2)) fulfil the coordination requirements of Co(1) resulting in a $\{N_2O_4\}$ chromophore. Meanwhile Co(2) ions present an O_6 donor set achieved through four oxygens (O(4), O(5), O(7), O(8)) from two bidentate nitrate anions and two alkoxide bridging oxygen atoms O(1), O′(3) (symmetry code: (′): $1-x, 2-y, 1-z$). The coordination bond distances for Co(1) lie in the range 1.884–1.991 Å, significantly shorter than Co(2) falling in the range 1.939–2.373 Å

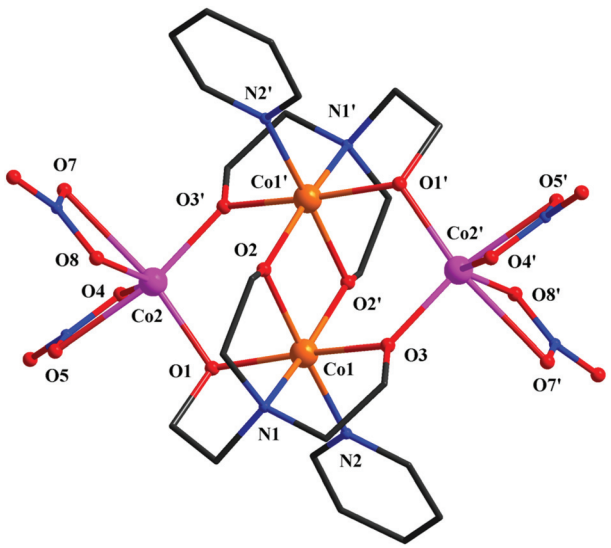

Fig. 1 Partially labelled plot of the structure of **1**. Hydrogen atoms have been omitted for clarity. Colour code: Co(II): magenta, Co(III): orange, O: red, N: blue, C: grey. Primed atoms are generated by symmetry (′) $1-x, 2-y, 1-z$.

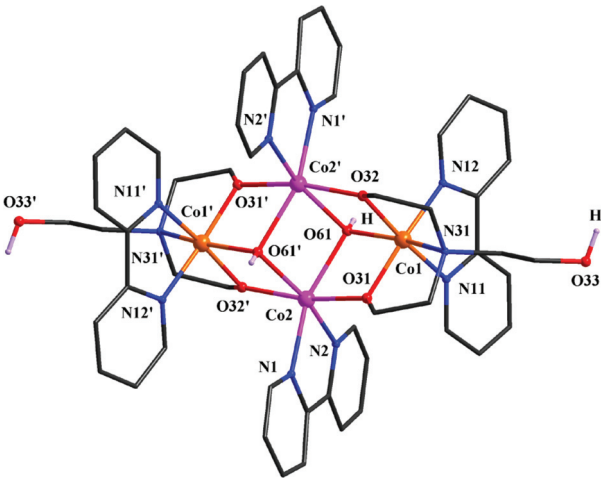

Fig. 2 Partially labelled plot of the tetranuclear cationic unit of **2**. Only the hydroxide hydrogen atoms are shown for clarity. Colour code: Co(II): magenta, Co(III): orange, O: red, N: blue, C: grey, H: light purple. Primed atoms are generated by symmetry (′) $-x, -y, -z$.

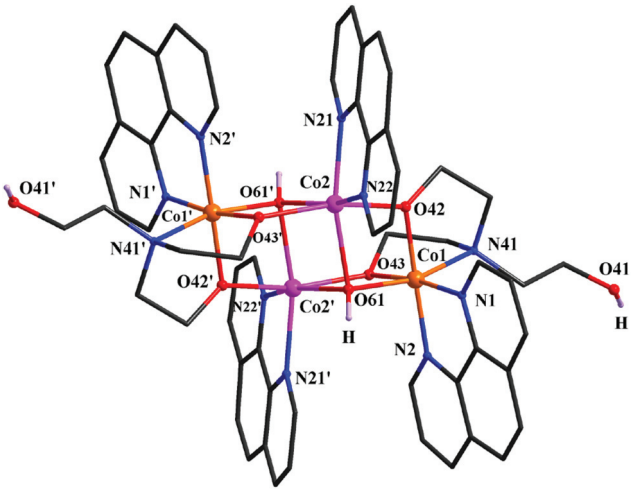

Fig. 3 Partially labelled plot of the tetranuclear cationic unit of **3**. Only the hydroxide hydrogen atoms are shown for clarity. Colour code: Co(II): magenta, Co(III): orange, O: red, N: blue, C: grey, H: light purple. Primed atoms are generated by symmetry (′) $-x, 2-y, -z$.

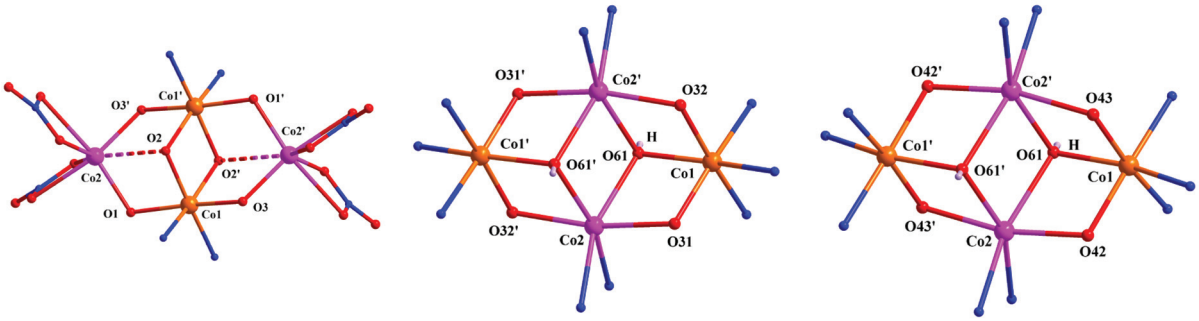

Fig. 4 Representation of the tetranuclear cores of complexes **1–3**. Colour code: Co(II): magenta, Co(III): orange, O: red, N: blue.

Table 2 Bond lengths [Å] and angles [°] in **1**, **2** and **3**[a]

Co(III) distances [Å]					
(**1**)		(**2**)		(**3**)	
Co1–O2	1.884(4)	Co1–O31	1.856(4)	Co1–O43	1.855(2)
Co1–O3	1.891(4)	Co1–O32	1.881(5)	Co1–O42	1.876(2)
Co1–N1	1.915(6)	Co1–O61	1.926(5)	Co1–O61	1.935(2)
Co1–O2′	1.922(5)	Co1–N12	1.940(6)	Co1–N2	1.948(2)
Co1–O1	1.921(5)	Co1–N11	1.944(6)	Co1–N1	1.954(2)
Co1–N2	1.991(5)	Co1–N31	1.980(6)	Co1–N41	1.985(3)
Co(II) distances [Å]					
Co2–O3′	1.939(5)	Co2–O32′	2.023(5)	Co2–O42	1.992(2)
Co2–O1	1.968(5)	Co2–O31	2.063(4)	Co2–O43′	2.072(2)
Co2–O4	2.073(5)	Co2–O61	2.108(6)	Co2–O61′	2.126(2)
Co2–O8	2.077(5)	Co2–N1	2.109(6)	Co2–N21	2.130(3)
Co2–O5	2.303(6)	Co2–N2	2.113(6)	Co2–N22	2.136(2)
Co2–O7	2.373(5)	Co2–O61′	2.155(5)	Co2–O61	2.189(2)
Angles					
(**1**)		(**2**)		(**3**)	
O2–Co1–O3	92.1(2)	O31–Co1–O32	94.1(2)	O43–Co1–O42	94.8(1)
O2–Co1–N1	88.3(2)	O31–Co1–O61	83.2(2)	O43–Co1–O61	83.3(1)
O3–Co1–N1	85.8(2)	O32–Co1–O61	82.5(2)	O42–Co1–O61	82.2(1)
O2–Co1–O2′	80.4(2)	O32–Co1–N12	92.3(3)	O42–Co1–N2	175.2(1)
O3–Co1–O2′	85.6(2)	O31–Co1–N12	172.8(2)	O43–Co1–N2	89.5(1)
N1–Co1–O2′	165.6(2)	O31–Co1–N11	91.1(2)	O43–Co1–N1	172.0(1)
O2–Co1–O1	86.7(2)	O32–Co1–N11	174.3(2)	O42–Co1–N1	92.3(1)
O3–Co1–O1	171.4(2)	O61–Co1–N12	94.5(2)	O61–Co1–N2	96.3(1)
N1–Co1–O1	85.6(2)	N12–Co1–N11	82.3(3)	N1–Co1–N2	83.3(1)
O2′–Co1–O1	102.5(2)	O31–Co1–N31	86.7(2)	O43–Co1–N41	87.6(1)
O2–Co1–N2	171.2(2)	O61–Co1–N11	95.9(2)	O61–Co1–N1	94.2(1)
O3–Co1–N2	92.0(2)	O32–Co1–N31	86.6(2)	N2–Co1–N41	96.6(1)
N1–Co1–N2	99.7(2)	N12–Co1–N31	97.0(2)	N1–Co1–N41	96.5(1)
O2′–Co1–N2	92.2(2)	O61–Co1–N31	164.5(2)	O42–Co1–N41	85.7(1)
O1–Co2–N2	90.4(2)	N11–Co1–N31	96.0(2)	O61–Co1–N41	164.1(1)
O3′–Co2–O1	103.6(2)	O32′–Co2–O61	100.9(2)	O42–Co2–O43′	167.4(1)
O3′–Co2–O4	97.8(2)	O31–Co2–O61	74.0(2)	O43′–Co2–O61′	73.8(1)
O1–Co2–O4	102.6(2)	O32′–Co2–N1	99.0(2)	O42–Co2–N21	91.0(1)
O3′–Co2–O8	108.2(2)	O32′–Co2–N2	89.4(2)	O61′–Co2–N21	96.2(1)
O1–Co2–O8	109.0(2)	O32′–Co2–O31	167.7(2)	O43′–Co2–N22	86.7(1)
O4–Co2–O8	132.2(2)	O32′–Co2–O61′	73.8(2)	O42–Co2–O61′	101.0(1)
O3′–Co2–O5	154.5(2)	O31–Co2–N1	87.2(2)	N21–Co2–N22	77.8(1)
O1–Co2–O5	91.3(2)	N1–Co2–O61′	103.9(2)	O43′–Co2–N21	100.9(1)
O4–Co2–O5	58.2(2)	O61–Co2–N1	159.8(2)	O43′–Co2–O61	94.6(1)
O8–Co2–O5	85.7(2)	O31–Co2–N2	102.4(2)	O61′–Co2–O61	86.0(1)
O3′–Co2–O7	87.8(2)	O61–Co2–N2	98.6(2)	O42–Co2–N22	100.1(1)
O1–Co2–O7	164.9(2)	N1–Co2–N2	77.8(2)	O61′–Co2–N22	158.2(1)
O4–Co2–O7	85.4(2)	N2–Co2–O61′	163.3(2)	O42–Co2–O61	73.4(1)
O8–Co2–O7	57.2(2)	O31–Co2–O61′	94.4(2)	N21–Co2–O61	164.4(1)
O5–Co2–O7	82.0(2)	O61–Co2–O61′	85.3(2)	N22–Co2–O61	105.5(1)

[a] Symmetry transformations used to generate equivalent atoms: **1:** (′) $1-x, 2-y, 2-z$; **2:** (′) $-x, -y, -z$; **3:** (′) $-x, 2-y, -z$.

indicating the presence of mixed valence cobalt ions (Co(1) as Co^{III} and Co(2) as Co^{II}). Moreover, assignment of oxidation states was determined by inspection of metric parameters and confirmed by bond-valence sum (BVS) analysis developed by Brown and Thorp and co-workers.[40] The BVS values found for Co(1) = 3.14, and Co(2) = 2.05, respectively; thus confirmed that Co^{III} corresponds to Co(1) ions and Co^{II} to Co(2) ions. The four cobalt atoms are located at a plane, generating an approximate Co_4 rhombus with two pairs of almost equal edge distances [3.353 Å and 3.307 Å]. Interatomic Co···Co separations found in the order Co(III)–Co(III) (2.907 Å) < Co(III)–Co(II) (mean distance 3.33 Å) < Co(II)–Co(II) (5.992 Å) and are in agreement with mixed valence tetranuclear structures with Co^{III}–Co^{III} internal positions.[24,27]

The bridging central core angle Co(1)–O(2)–Co′(1) is 99.6(2)° significantly shorter than the external bond angles Co(1)–O(3)–Co′(2) 122.2(2)° and Co(2)–O(1)–Co(1) 116.5(3)° as a result of the imperfectness of **1**.

Structure analysis of $[Co^{II}_2Co^{III}_2(\mu_3\text{-}OH)_2(Htea)_2(bpy)_4](NO_3)_4$ (2), and $[Co^{II}_2Co^{III}_2(\mu_3\text{-}OH)_2(Htea)_2(phen)_4](NO_3)_4\cdot 2CH_3CN\cdot 2CH_3OH$ (3)

DIAMOND diagrams of the crystal structures of **2** and **3** appear in Fig. 2 and 3, respectively and selected bond distances and angles are listed in Table 2. The tetranuclear cationic units in **2** and **3** as structural analogues are discussed together. In both structures two μ_3-hydroxo bridges occur, providing O(61) to connect the central Co(2) ions with the external Co(1) ions. Even though the μ_3-hydroxo bridge is common in coordination chemistry, it has not yet been observed in any of the reported tetranuclear mixed valence cobalt clusters, thus **2** and **3** are the first evidence of such coordination pattern. Each structure is stabilized by four NO_3^- counteranions. The doubly deprotonated triethanolamine (Htea) acts in a 3.2201 fashion.[39] The alkoxide oxygens O(31) and O(32) for **2** and O(43) and O(42) for **3** are bridging the internal Co(2) ions with the external Co(1) ions, while one alkoxide arm of the tripodal remains uncoordinated (O(33) for **2** and O(41) for **3**).

All cobalt ions are in octahedral configuration. The external Co(1) has a $\{N_3O_3\}$ chromophore composed of a hydroxide oxygen (O(61)), two alkoxide oxygens (O(32) and O(31) for **2** and O(43) and O(42) for **3**), a nitrogen from the tripodal (N(31) for **2** and N(41) for **3**) and two nitrogen atoms coming from the N,N-donors (N(11), N(12) for **2** and N(1), N(2) for **3**).

The central Co(2) has a $\{N_2O_4\}$ chromophore composed of two alkoxide oxygens from the Htea ligand O(31), O′(32) (symmetry code (′): $-x, -y, -z$) for **2** and O(42), O′(43) (symmetry code (′): $-x, 2-y, -z$), for **3**, one hydroxide oxygen atom [O′(61) for **2** and for **3**] and two nitrogens N(1), N(2) of bpy for **2** and N(21), N(22) of phen donors for **3**, respectively. Bond distances of Co(1) found almost identical to both structures and lie in the range of 1.856–1.980 Å for **2** and 1.856–1.985 Å for **3**, significantly shorter than of Co(2) 2.023–2.155 Å for **2** and 1.992–2.188 Å for **3** indicating mixed valence compound. In addition, BVS analysis showed for Co(1) = 3.25/3.21 and Co(2) = 1.96/1.92 for **2** and **3** respectively; thus confirmed that Co^{III} corresponds to Co(1) ions and Co^{II} to Co(2) ions. It is also to be noted that the charge arrangements as described above fully agrees with the magnetic properties of **2** and **3**.

As in **1** the four cobalt atoms are located at a plane, generating an approximate Co_4 rhombus with two pairs of almost equal edge distances [3.076 Å and 3.097 Å for **2**; 3.092 Å and 3.105 Å for **3**]. Moreover, the Co···Co separations in **2** and **3**, due to reversal distribution of the cobalt ions compared to **1**, follow an opposite order; Co(III)–Co(III) (5.318/5.334 Å) > Co(III)–Co(II) (mean distance 3.086/3.098 Å) > Co(II)–Co(II) (3.135/3.155 Å) and are in good agreement with the values found before for analogous cubane-like complexes with Co^{II}–Co^{II} internal positions.[22,23,25,26] The mean N,N-donor plane coordinated to Co^{III} is inclined to the cobalt ions mean plane by an angle of 53.9/53.5° in **2** and **3**, respectively. The corresponding angles involving the N,N-donors coordinated to Co^{II} are 76.2/72.8° in **2** and **3**, respectively.

The internal Co(2)–O(61)–Co′(2) angle found almost the same 94.7(2)° for **2** and 94.0(1)° for **3** respectively, smaller than **1** as expected due to the nature of the hydroxide bridge.

The nitrate counterions are linked to the cationic cluster in **2** through strong inter-molecular hydrogen bonding interactions involving the free alkoxide group of each Htea and the two hydroxide bridges (Fig. 5) [O(33)···O(51) = 2.733 Å, H(33O)···O(51) = 2.196 Å, O(33)–H(33O)···O(51) = 121.7°; O(61)···O(42) ($-x, -y, -z$) = 2.792 Å, H(61O)···O(42) = 2.151 Å, O(61)–H(61O)···O(42) = 166.8°]. On the other hand, the lattice structure of **3** is completely different, although generated by similar inter-molecular hydrogen bonding interactions, involving the free alkoxide group of each Htea and the two hydroxide bridges [O(41)···O(52) = 2.781 Å, H(41O)···O(52) = 1.999 Å, O(41)–H(41O)···O(52) = 162.9°; O(61)···O(53) ($-1+x, y, z$) = 2.873 Å, H(61O)···O(53) = 1.913 Å, O(61)–H(61O)···O(53) = 161.9°] which link the tetranuclear cations into 1D chains along the crystallographic *a*-axis (Fig. 6).

Magnetics and EPR

Two different theoretical models were used to investigate the magnetic behavior of compound **1**. The first model (isotropic

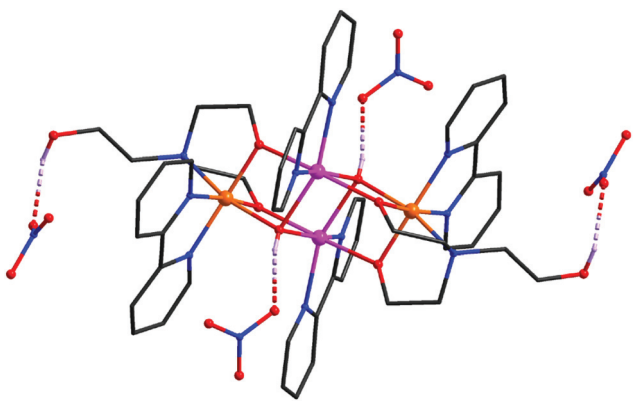

Fig. 5 Inter-molecular H-bonding interactions (dashed lines) in **2**. Colour code: Co(II): magenta, Co(III): orange, O: red, N: blue, C: grey, H: light purple.

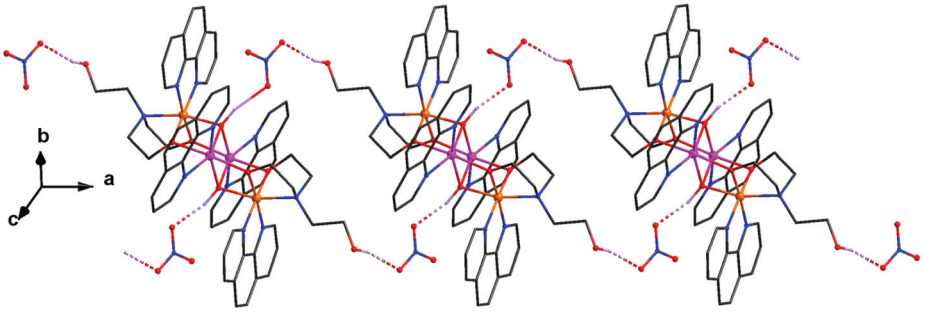

Fig. 6 A small fragment of the 1D lattice structure in **3** along the *a*-axis due to inter-molecular H-bonding interactions (dashed lines). Colour code: Co(II): magenta, Co(III): orange, O: red, N: blue, C: grey, H: light purple.

Heisenberg model with local anisotropy terms – see eqn (4) below) takes into account (i) both the axial and rhombic parts of distortion of the crystal field (D, E), (ii) an isotropic g-value, and (iii) the isotropic spin–spin interaction between the two magnetic centers ($S_1 = S_2 = 3/2$).[41] The second model (anisotropic Heisenberg Hamiltonian – see eqn (5) below) is applied in the low temperature range ($T < 40$ K)[42,43] where only the low-lying anisotropic spin-doublet $S = 1/2$ is populated. This effective spin doublet arises from the splitting of the $^4T_1$ term through spin–orbit coupling and local distortion of the octahedral sites. According to the anisotropic model: (a) the effective spin is $S_1 = S_2 = 1/2$, and (b) there are axial exchange interaction terms J ($J_x = J_y$, J_z) and g ($g_x = g_y$, g_z). It should be noted here that for $J_z \neq 0$ and $J_x = J_y = 0$, the system is in the Ising limit while for $J_z = 0$ and $J_x = J_y \neq 0$, the system is in the XY limit.

$$H = -JS_1S_2 + D\left[S_z^2 - \frac{1}{3}S(S+1)\right] + E\left(S_x^2 - S_y^2\right) + B g_i S_i \quad (4)$$

$$H = -\left(J_z S_1^z S_2^z + J_x S_1^x S_2^x + J_y S_1^y S_2^y\right) + B g_i S_i \quad (5)$$

Magnetic properties of compound 1

Magnetic susceptibility measurements were carried out at different magnetic fields and in the temperature range 2–300 K. Fig. 7 shows the $\chi_M T$ per 2Co(II) ions *versus* T susceptibility data at 0.1 T for compound **1**. The $\chi_M T$ values decrease smoothly from 5.5 emu mol^{-1} K at 300 K to 5.0 emu mol^{-1} K at 70 K and then more steeply to a minimum value of 1.3 emu mol^{-1} K at 2 K. The high-temperature value of $\chi_M T$ is higher than 3.75 emu mol^{-1} K, the value that would be expected for two Co(II) ions with an $S = 3/2$. This behavior is consistent with the presence of a significant orbital contribution to the anisotropic nature of the Co(II) system investigated while the low temperature decrease of the susceptibility data is due to antiferromagnetic exchange interaction between the Co(II) ions and zero-field interactions.

While the significance of the exchange interaction between the magnetic Co(II) centers is not obvious for compound **1**, fitting attempts without the spin–spin interaction ended up with unrealistic results or unacceptable agreement factors concerning the fitting processing. The fitting results using eqn (4)

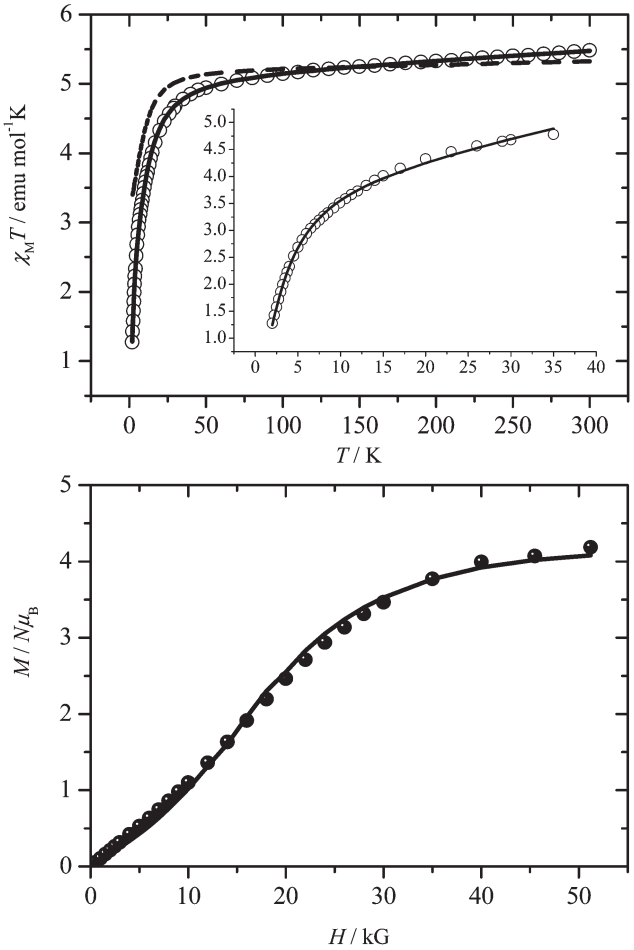

Fig. 7 Temperature dependence of the susceptibility data of complex **1** in the form of $\chi_M T$ per 2Co(II) ions *versus* T at 0.5 T. Solid line and stars are theoretical curves according to different Hamiltonian equations (see text for details).

yield the following parameters: $J = 2.0(2)$ cm^{-1}, $g = 2.35(1)$, $D = 11.0(1)$ cm^{-1} and the theoretical curve is shown in Fig. 7 as a solid line. In the same figure another simulation is carried out (dotted line) where the exchange interaction part was set to zero ($J = 0$) in order to point out its significance. The sign of the D parameter along with the E parameter were not resolved from the magnetic measurements, while introduction of an axial symmetry to the g-parameter ($g_\perp$, $g_{||}$) leads to no

improvement of the fit. The value of the D parameter is in accordance with an octahedral Co(II).[44]

The relatively strong next-nearest-neighbor antiferromagnetic exchange interaction is not unrealistic when the centers are connected *via* diamagnetic metal ions with low electron-promotion energies between neighboring metals. This is the case also of an investigated heteronuclear complex $[Fe^{III}Co^{III}Fe^{III}]^{3+}$ in which a relatively low electron-promotion energy between cobalt and iron sites is present.[45] Another example is the Prussian blue molecular magnet, in which the interaction between next-nearest-neighbor high-spin Fe(III) sites is mediated by a bridge containing the diamagnetic Fe(II) ion.

The best fit of the experimental susceptibility data to the expression for the magnetic susceptibility derived from eqn (5), gives the following exchange parameters $J_z = -7.1(2)$ cm^{-1}, $g_z = 6.8(1)$, $J_{xy}/J_z = 0.34(2)$, and $g_{xy}/g_z = 0.52(2)$ and is shown as a solid line in the inset of Fig. 7 along with the experimental points (open cycles). If we have in mind that $J_{iso} = (J_x + J_y + J_z)/3$, then the value of isotropic exchange constant J_{iso} for this model is $J_{iso} = -4.0(2)$ cm^{-1}, which is in accordance with a small anisotropic antiferromagnetic interaction and close to the value obtained from the model described in eqn (4). To test the validity of the fitting values, the magnitude of the anisotropy for the Co–Co interaction was investigated. Generally, that is given by $J_{xy}/J_z \sim (g_{xy}/g_z)^2$, where J_{xy} and J_z are the parallel and perpendicular exchange components to the spin direction (J has been assumed to be axial).[43,46] On the basis of the values obtained from the fitting process, an agreement arises between the two terms of the aforementioned mathematical relationship.

Magnetization measurements on **1** were carried out at 2 K, and in the field range 0–5 T. The derived data are shown in the form of M/N [μ_B] *vs.* H [kG] in Fig. 7. To further investigate the fitting process, simulations of the magnetization data (*vide infra*) were carried out using the values obtained from the susceptibility fitting. The results are also shown in Fig. 7 as solid lines. Here too, the observed simulation is in agreement with the experimental curve.

It should be mentioned here that the anisotropic model gave an exchange interaction term (J_{iso} value) which is larger from the value found from the model described with eqn (4). Thus, it is difficult to correlate the results due to the different nature of the two aforementioned models.

Magnetic susceptibility for 2 and 3

Magnetic susceptibility measurements were carried out at different magnetic fields and in the temperature range 2–300 K. Fig. 8 and 9 shows the $\chi_M T$ per 2Co(II) ions *versus* T susceptibility data at 0.1 T for complexes **2** and **3** respectively, while the solid lines represent the fit according to the general Hamiltonian in eqn (4). The $\chi_M T$ values increase smoothly from 6.0 (6.5) emu mol^{-1} K at 300 K to a maximum value of 7.3 (7.7) emu mol^{-1} K at 10 K while an abrupt decrease follows to the value of 6.4 (6.7) at 2 K. The high-temperature value of $\chi_M T$ is higher than 3.75 emu mol^{-1} K, the value that would be

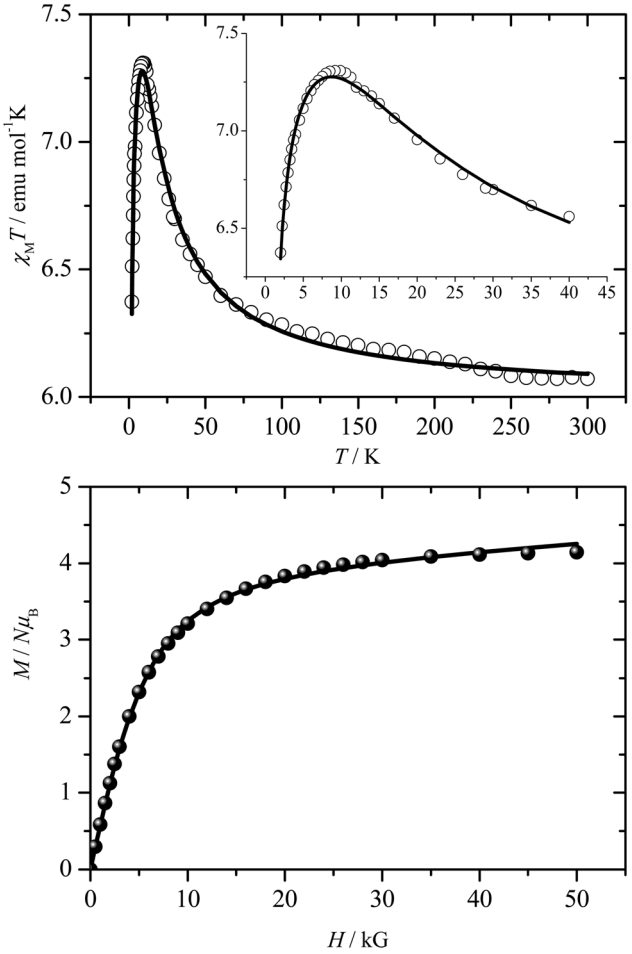

Fig. 8 Temperature dependence of the susceptibility data of complex **2** in the form of $\chi_M T$ per 2Co(II) ions *versus* T at 0.5 T. Solid line and stars-line are theoretical curves according to different Hamiltonian equations (see text for details).

expected for two Co(II) ions with an $S = 3/2$. This behavior is consistent with the presence of a significant orbital contribution to the anisotropic nature of the Co(II) system investigated while the increase of the data is due to ferromagnetic interaction between the Co(II) ions. The abrupt low temperature decrease (for temperatures lower than 10 K) of the susceptibility data is due to zero field/intermolecular interactions. The fitting results are: $J = 3.2(2)/3.8(2)$ cm^{-1}, $D = 8.5(1)/7.8(1)$ cm^{-1}, $g = 2.52(1)/2.57(1)$ cm^{-1} for **2** and **3**, respectively.

In order to investigate the anisotropic nature of the exchange interaction between the Co(II) ions a Hamiltonian formalism (eqn (5)) was used and an analogous fitting procedure as described previously was carried out. The fitting results for **2** and **3** are shown as solid lines in the inset of the susceptibility plot (upper plot in Fig. 8 and 9) and the values are: $J_z = 19.2(2)/22.1(2)$ cm^{-1}, $g_z = 8.1(1)/8.3(1)$, $J_{xy}/J_z = 0.11(2)/0.14(2)$, and $g_{xy}/g_z = 0.28(2)/0.36(2)$, respectively. The obtained isotropic exchange interaction values for **2** and **3** are: $J_{iso} = 7.6(2)/9.3(2)$ cm^{-1}.

Magnetization measurements on **2** and **3** were carried out at 2 K, and in the field range 0–5 T. The derived data are

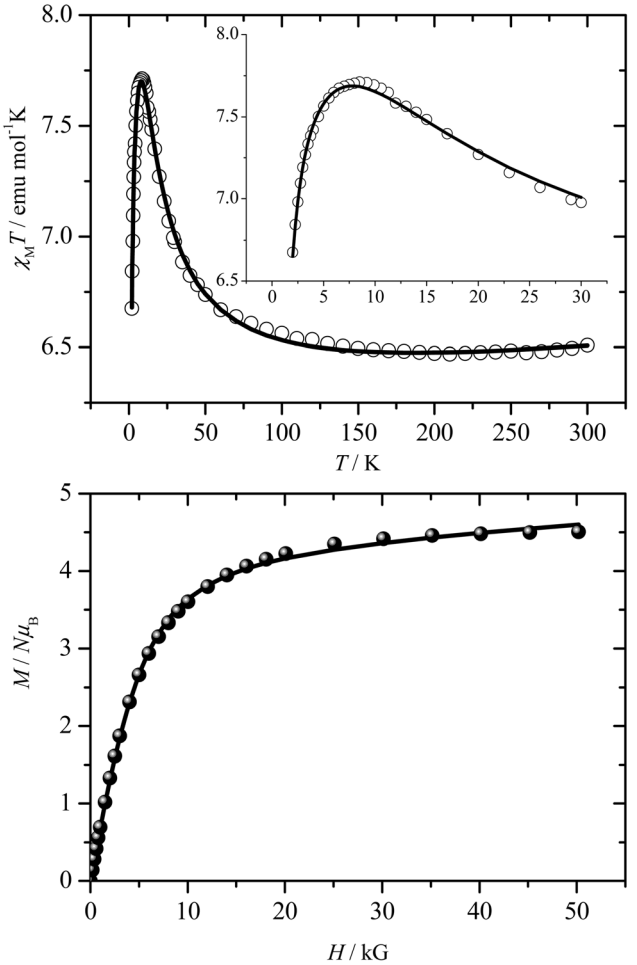

Fig. 9 Temperature dependence of the susceptibility data of complex **3** in the form of $\chi_M T$ per 2Co(II) ions *versus* T at 0.5 T. Solid line and stars-line are theoretical curves according to different Hamiltonian equations (see text for details).

shown in the form of M/N [μ_B] *vs.* H [kG] in Fig. 8 and 9, respectively. To further investigate the fitting process, simulations of the magnetization data (*vide infra*) were carried out using the values obtained from the susceptibility fitting. The results are also shown in the same figures as solid lines while the observed simulations are in agreement with the experimental curves.

Also for these two compounds the anisotropic models gave exchange interaction terms (J_{iso} value) which are larger than the value found from the model described with eqn (4) but of the same magnitude.

Comments on the magnetostructural criteria

It would be desirable for rationalizing the observed magnetic properties, to establish a correlation with the structure parameters that governs the synthesis of the tetranuclear cubane-like cobalt clusters. Such a correlation would be also useful to assist in the rational design of complexes with specific magnetic properties such as large spin ground states. Although such correlations have been established for dinuclear systems such as hydroxide-bridged dicopper(II) complexes,[47] oxide-bridged dimanganese(IV) complexes,[48] and phenoxide-bridged dinickel(II) complexes,[49] the case of dinuclear Co(II) systems is still open due to the difficulty arises from the anisotropic nature of the Co(II) ion.

In order to give a physical meaning to the derived J values, we tried to correlate the structural parameters and the magnetic behavior displayed in tetranuclear mixed valence cubane-like clusters where Co^{II} ions form the central core. Thus, we examined (a) the distance between the metallic centers Co(II)···Co(II), and (b) the angle Co–O–Co (φ) due to the nature of the μ-OR bridge (HO^- or RO^-) along the short diagonal in compounds **2** and **3** and in analogous tetranuclear cubane-like clusters. The data are listed in Table 3. The correlation indicates that as the Co–O–Co angle increases, the antiferromagnetic behavior becomes stronger until a certain value (~97°),[32] in which a system can show either weak ferromagnetic or weak antiferromagnetic behavior while the ferromagnetic behavior is clearly observed below the angle 97°. Therefore, a structural comparison between the complexes in Table 3 indicates that the Co···Co distance in **2** and **3**, is the shortest while the bridging Co–O–Co angle is the smallest; thus **2** and **3** are the only two examples displaying ferromagnetic interactions. When the Co–O–Co is higher than 97° the interaction becomes antiferromagnetic which is the case of two compounds listed in Table 3 (bridging angles are 98.37° and 99.39°, respectively) while for Co–O–Co angles close to 97° the interaction is either weak ferromagnetic or weak antiferromagnetic and represents the magnetic behavior of two other compounds listed in the same table.

These observations were expected most likely due to the nature of the bridge and its influence on the corresponding angles and bond distances. In so doing, a relationship between the exchange interaction constant and a parameter related to Co–O–Co angles in alkoxide-bridge complexes of dicobalt units within polynuclear topologies, has been established and reported elsewhere by us.[32]

EPR spectroscopy

Compound 1. X-Band EPR measurements were carried out in powder samples of compound **1** and are shown in Fig. 10. As a consequence of the fast spin–lattice relaxation time of high-spin Co(II), signals were observed only below 70 K where a derivative centered at *ca.* g = 5.3 appears.

The dominant broadening effect emerges when the g-strain is converted into B-strain through the equation

$$\Delta B = -\left(\frac{h\nu}{\mu_B}\right)\left(\frac{\Delta g}{g^2}\right),$$

where the parameters have their usual meaning. Thus, the largest and smallest g-values of the powder spectra have field widths that differ by an order of magnitude, thereby rationalizing the broad high-field features of the spectrum.

Compounds 2 and 3. To explore the existence of a weak interaction between the Co(II) centers in the case of compounds **2** and **3**, X-band powder EPR experiments were carried out in the temperature range 4–40 K (Fig. 11). As a

Table 3 Selected magnetostructural data for tetranuclear mixed valence cubane-like clusters with central Co^{II} ions[a]

Tetranuclear clusters of mixed valence cores	$Co^{II}\cdots Co^{II}$ (Å)	Co–O–Co, φ (°)	Type of bridge (RO^-)	Magnetic behavior	Ref.
$[Co_4(\mu_3\text{-}OH)_2(Htea)_2(bpy)_4](NO_3)_4$ (**2**)	3.13	94.64	μ_3-OH	F (J_z = 19.2(2) and J_{xy} = 0.11(2) cm^{-1})	Our work
$[Co_4(\mu_3\text{-}OH)_2(Htea)_2(phen)_4](NO_3)_4\cdot 2MeCN\cdot 2MeOH$ (**3**)	3.15	94.00	μ_3-OH	F (J_z = 22.1(2) and J_{xy} = 0.14(2) cm^{-1})	Our work
$[Co_4(C_{14}H_{19}O_3N_2)_2(\mu_3\text{-}OMe)_2(NO_3)(H_2O)_2](NO_3)\cdot 2(H_2O)$	3.18	96.6/99.1	CH_3O–	Weak F (J_z = 8.51 and J_{xy} = 0.45 cm^{-1})	25
$[Co_4\{NH(C_2H_4OH)_2\}_2\{NH(C_2H_4O)_2\}_4](ClO_4)$	3.29	97.2	RCH_2O–	Weak AF	23
$[Co_4(\mu_{1,1}\text{-}N_3)_4(N_3)_2(HDMSP)_2(MeOH)_2]\cdot 2H_2O$	3.19	98.37	RCH_2O–	AF (J = −5.94 cm^{-1})	26
$[Co_4(H_2hbhpd)_2(H_4hbhpd)_2(H_2O)_2]\cdot Cl_2\cdot (MeOH)_4$	3.22	99.39	RCH_2O–	AF	22

[a] H_3DMSP = 1,3-dihydroxy-2-methyl-2-(salicylideneamino)propane; H_5hbhpd = 2-(2-hydroxy-benzylamino)-2-hydroxymethyl-propane-1,3-diol.

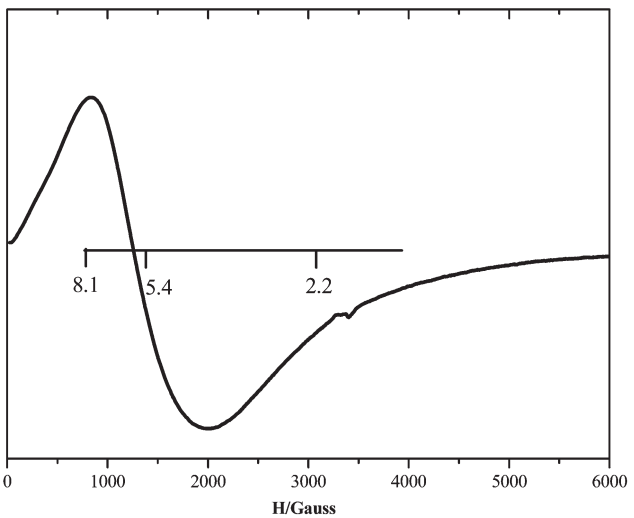

Fig. 10 Powder X-Band EPR spectra of complex **1** at 4 K.

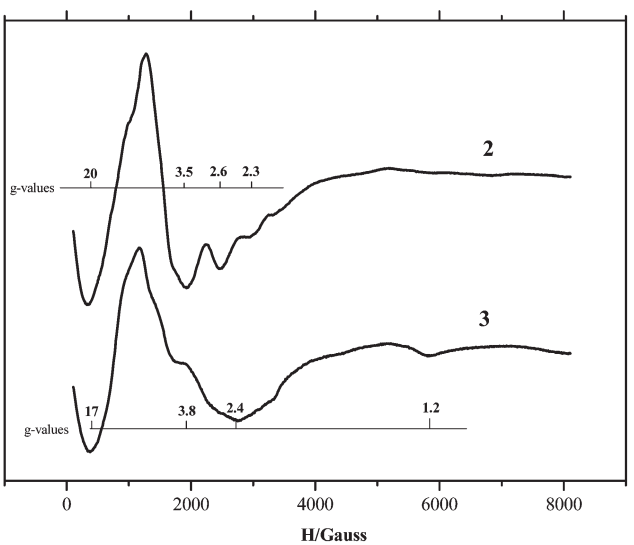

Fig. 11 Powder X-Band EPR spectra of complexes **2** and **3** at 4 K.

consequence of the fast spin–lattice relaxation time of high-spin Co(II), signals were observed only below 40 K. The g values obtained from the powder EPR spectrum show large variations in the range 20.0–1.0 which is an indication of an exchange interaction between the Co(II) ions.

An important piece of information pertaining to the nature of the exchange interaction emerges from the g values of the single cobalt(II) ion. Therefore, if $g_z > g_x, g_y$, then the ion is closer to the Ising limit. Or, if $g_x, g_y > g_z$, then the system is closer to the XY limit. The conditions for observing $g_z > g_x, g_y$ were given earlier by Abragam and Bleaney, using a crystal field approach.[46] In that respect, it was found that in the Ising limit g_z = 8–9 and $g_x = g_y = 0$, while for the XY limit g_{xy} = 4 and g_z = 2. The values observed here for **2** and **3** are beyond every limit, thus indicating that an interaction between the two Co(II) octahedral centers does arise.

Conclusions

Three new members were added to the defective dicubanes family of $Co^{II/III}$ chemistry. Two different models were used to investigate the magnetic behavior of these compounds: (i) an isotropic model (concerning the exchange interaction constants) with local anisotropic terms (zero field splitting, D) employed in the whole temperature range and (ii) an anisotropic one with axial exchange interaction terms employed in the low temperature range T < 30 K. Although there is no coincidence concerning the absolute values of the exchange interaction constants derived from the previous models, further investigation of this methodology for the magnetic study of polynuclear Co(II) complexes is mandatory in order to derive possible correlations between the two different models. Furthermore it is shown that there is a correlation between the sign and magnitude of the magnetic exchange interaction constant and the Co–O–Co angle with a turning point from ferromagnetic to antiferromagnetic behavior at around 97°. This observation needs further clarification and a quantitative study of many polynuclear Co(II) complexes in order to derive an appropriate equation between the magnitude of the

J constant and the Co–O–Co angle and the proposed magnetic methodology can play an important role.

Experimental

Materials and methods

All experiments were carried out under aerobic conditions. All chemicals and solvents were of reagent grade. Triethanolamine, $Co(NO_3)_2{\cdot}6H_2O$, pyridine, 2,2′-bipyridine, 1,10-phenanthroline, triethylamine, CH_3OH and CH_3CN were purchased from Aldrich Chemical Co., Milwaukee, WI (USA) and used without further purification.

Physical measurements

FT-Infrared spectra (200–4000 cm^{-1}) were recorded on a NICOLET 6700 FT-IR spectrometer with samples prepared as KBr pellets. C, H and N elemental analysis was performed on a Perkin-Elmer 240B elemental analyzer.

The EPR spectra in the solid state were recorded on a Bruker ER 200D-SRC X-band spectrometer, equipped with an Oxford ESR 9 cryostat, operating at 9.61 GHz, 10 dB (2 mW) and at 4 K. Magnetic susceptibility data were collected on powdered samples with a Quantum Design SQUID susceptometer in the 2–300 K temperature range, under various applied magnetic fields. Magnetization measurements were carried out at three different temperatures in the field range 0–5 T.

X-Ray crystal structure determination

Crystals of **1** (0.06 × 0.13 × 0.17 mm), **2** (0.03 × 0.35 × 0.42 mm), and **3** (0.08 × 0.28 × 0.35 mm) were taken from the mother liquor and immediately cooled to −113 °C. Diffraction measurements were made on a Rigaku R-AXIS SPIDER image plate diffractometer using graphite monochromated Cu-Kα radiation. Data collection (ω-scans) and processing (cell refinement, data reduction and empirical/numerical absorption correction) were performed using the CrystalClear program package.[50] The structure was solved by direct methods using SHELXS-97[51] and refined by full-matrix least-squares techniques on F^2 with SHELXL-97.[52] Important crystallographic data are listed in Table 1. Hydrogen atoms were either located by difference maps and were refined isotropically or were introduced at calculated positions as riding on bonded atoms. Hydrogen atoms for the MeOH solvated molecules in **3** were not included in the refinement. All non-hydrogen atoms were refined anisotropically.

Synthesis of the compounds

General procedure. 0.56 mmol (0.163 g) of $Co(NO_3)_2{\cdot}6H_2O$ were dissolved in MeOH (20 mL) and then a mixture of 0.56 mmol of the N-donor, 0.56 mmol (0.084 g) of H_3tea and 1.7 mmol (0.17 g) of Et_3N, was dissolved in MeOH (10 mL), and added to the initial solution. The reaction mixture was left under stirring for 1 h. The obtained red-brown solution was filtered and then 10 mL of MeCN were added to the filtrate.

Table 1 Summary of crystal, intensity collection and refinement data for $[Co^{II}_2Co^{III}_2(tea)_2(pyr)_2(NO_3)_4]{\cdot}2CH_3CN$ (**1**), $[Co^{II}_2Co^{III}_2(\mu_3\text{-}OH)_2(Htea)_2(bpy)_4](NO_3)_4$ (**2**) and $[Co^{II}_2Co^{III}_2(\mu_3\text{-}OH)_2(Htea)_2(phen)_4](NO_3)_4{\cdot}2CH_3CN{\cdot}2CH_3OH$ (**3**)

	(**1**)	(**2**)	(**3**)
Formula	$C_{26}H_{40}Co_4N_{10}O_{18}$	$C_{52}H_{60}Co_4N_{14}O_{20}$	$C_{66}H_{74}Co_4N_{16}O_{22}$
Formula weight	1016.40	1436.86	1679.13
Temperature (°K)	160(2)	160(2)	160(2)
Wavelength	Cu K_α 1.54178	Cu K_α 1.54178	Cu K_α 1.54178
Space group	$P\bar{1}$	$P2_1/c$	$P2_1/c$
a (Å)	8.5625(1)	12.0397(2)	11.3408(2)
b (Å)	10.6064(1)	17.0443(3)	26.0914(4)
c (Å)	11.8189(2)	13.8828(2)	13.6498(2)
α (°)	112.827(1)	90.00	90.00
β (°)	91.391(1)	90.60(10)	116.305(1)
γ (°)	105.322(1)	90.00	90.00
V (Å^3)	944.38(2)	2848.71(8)	3620.7(1)
Z	1	2	2
D_{calcd}, (Mg m^{-3})	1.787	1.675	1.540
Abs. coeff. (μ), mm^{-1}	14.313	9.746	7.791
Range of h, k, l	$-10 \le h \le 10$ $-12 \le k \le 12$ $-12 \le l \le 13$	$-12 \le h \le 13$ $-18 \le k \le 19$ $-15 \le l \le 15$	$-9 \le h \le 13$ $-30 \le k \le 30$ $-16 \le l \le 16$
Goodness-of-fit on F^2	1.055	1.081	1.052
R^a	$R = 0.0777^b$	$R = 0.0736^b$	$R = 0.0470^b$
R_w [a]	$R_w = 0.1792^b$	$R_w = 0.1857^b$	$R_w = 0.1296^b$

[a] R values are based on F values, R_w values are based on F^2.

$$R = \frac{\sum ||F_o| - |F_c||}{\sum (|F_o|)}, \quad R_w = \sqrt{\frac{\sum \left[w(F_o^2 - F_c^2)^2\right]}{\sum \left[w(F_o^2)^2\right]}}$$

[b] For 2247 (**1**), 2566 (**2**) and 5445 (**3**) reflections with $I > 2\sigma(I)$.

For the synthesis of $[Co^{II}_2Co^{III}_2(tea)_2(pyr)_2(NO_3)_4]{\cdot}2MeCN$ (1). 0.044 g (0.56 mmol) of pyr was used while red-brown crystals suitable for X-ray structure determination were deposited by layering with diethyl ether after 2 days. Yield: 20%. (Fw = 1016.40). (Found: C, 31.20; H, 3.72; N, 13.67; $C_{26}H_{40}O_{18}N_{10}Co_4$ requires C, 31.57; H, 3.92; N, 13.72); IR: ν_{max}/cm^{-1}; ν_{as}(C–H): 2980 (w); ν_{sym}(C–H): 2926 (w); ν(C–N): 1607 (w); ν_{as}(–ONO_2): 1479 (m); ν_{sym}(–ONO_2): 1299 (m); ν(C–O): 1076 (w); 1047 (s); 1025 (w); (KBr pellet).

For the synthesis of $[Co^{II}_2Co^{III}_2(\mu_3\text{-}OH)_2(teaH)_2(bipy)_4](NO_3)_4$ (2). 0.087 g (0.56 mmol) bipy was used. Brown crystals of **2** suitable for X-ray structure determination were deposited by diethyl ether diffusion after 2 days. Yield: 75%. (Fw = 1436.86). (Found: C, 43.47; H, 4.21; N, 13.66; $C_{52}H_{60}O_{20}N_{14}Co_4$ requires C, 43.42; H, 4.18; N, 13.64); IR: ν_{max}/cm^{-1}; ν(O–H): 3420 (m, br); ν_{as}(C–H): 2970 (w); ν_{sym}(C–H): 2926 (w); ν(C–N): 1610 (w); $\nu(NO_3)$: 1384 (s); ν(C–O): 1092 (m); 1047 (m); 1020 (w) (KBr pellet).

For the synthesis of $[Co^{II}_2Co^{III}_2(\mu_3\text{-}OH)_2(teaH)_2(phen)_4](NO_3)_4{\cdot}2MeCN{\cdot}2MeOH$ (3). 0.1 g (0.56 mmol) phen was used. Dark brown crystals of **3** suitable for X-ray structure determination were deposited by layering with diethyl ether the next day. Yield: 60%. (Fw = 1679.13). (Found: C, 47.77; H, 4.13; N, 13.40; $C_{66}H_{74}Co_4N_{16}O_{22}$ requires C, 47.21; H, 4.44; N, 13.35); IR: ν_{max}/cm^{-1}; ν(O–H): 3404 (m, br); ν_{as}(C–H): 2980 (w); ν_{sym}(C–H): 2936 (w); ν(C–N) (w): 1625; $\nu(NO_3)$: 1384 (s); ν(C–O): 1092 (m); 1047 (m); 1036 (w); (KBr pellet).

References

1 For example, see: (*a*) R. E. P. Winpenny, *Chem. Soc. Rev.*, 1998, **27**, 447; (*b*) U. Riaz, O. J. Curnow and M. D. Curtis, *J. Am. Chem. Soc.*, 1994, **116**, 4357; (*c*) R. D. Adams and B. Captain, *Angew. Chem., Int. Ed.*, 2008, **47**, 252.

2 For example, see: (*a*) J. Koehler, A. C. J. Brouwer, E. J. J. Groenen and J. Schmidt, *Science*, 1995, **268**, 1457; (*b*) R. Bagai and G. Christou, *Chem. Soc. Rev.*, 2009, **38**, 1011; (*c*) D. Gatteschi and R. Sessoli, *Angew. Chem., Int. Ed.*, 2003, **42**, 268.

3 (*a*) S. Mukhopadhyay, S. K. Mandal, S. Bhaduri and W. H. Armstrong, *Chem. Rev.*, 2004, **104**, 3981; (*b*) G. Christou, *Acc. Chem. Res.*, 1989, **22**, 328.

4 For example, see: (*a*) C. Philouze, G. Blondin, J.-J. Girerd, J. Guilhem, C. Pascard and D. Lexa, *J. Am. Chem. Soc.*, 1994, **116**, 8557; (*b*) H. Chen, M.-N. Collomb, C. Duboc, G. Blondin, E. Rivière, J. W. Faller, R. H. Crabtree and G. W. Brudvig, *Inorg. Chem.*, 2005, **44**, 9567.

5 For example, see: (*a*) S. Shit, G. Rosair and S. Mitra, *J. Mol. Struct.*, 2011, **991**, 79; (*b*) G. Aromí, S. Badhuri, P. Artús, K. Folting and G. Christou, *Inorg. Chem.*, 2002, **41**, 805.

6 For examples see: (*a*) S. Wang, K. Folting, W. E. Streib, E. A. Schmitt, J. K. McCusker, D. N. Hendrickson and G. Christou, *Angew. Chem., Int. Ed. Engl.*, 1991, **30**, 305.

7 (*a*) E. S. Lang, R. Stieler and G. Manzoni de Oliveira, *Polyhedron*, 2010, **29**, 1760; (*b*) C. E. Dubé, S. Mukhopadhyay, P. J. Bonitatebus, R. J. Staples and W. H. Armstrong, *Inorg. Chem.*, 2005, **44**, 5161.

8 S. Mukhopadhyay, R. J. Staples and W. H. Armstrong, *Chem. Commun.*, 2002, 864.

9 (*a*) M. L. Kirk, M. K. Chan, W. H. Armstrong and E. I. Solomon, *J. Am. Chem. Soc.*, 1992, **114**, 10432; (*b*) S. Mukhopadhyay, H. J. Mok, R. J. Staples and W. H. Armstrong, *J. Am. Chem. Soc.*, 2004, **126**, 9202.

10 T. C. Stamatatos, S. Dionyssopoulou, G. Efthymiou, P. Kyritsis, C. P. Raptopoulou, A. Terzis, R. Vicente, A. Escuer and S. P. Perlepes, *Inorg. Chem.*, 2005, **44**, 3374.

11 For example, see: (*a*) E. C. Yang, D. N. Hendrickson, W. Wernsdorfer, M. Nakano, L. N. Zakharov, R. D. Sommer, A. L. Rheingold, M. Ledezma-Gairaud and G. Christou, *J. Appl. Phys.*, 2002, **91**, 7382; (*b*) M. Murrie, S. J. Teat, H. Stoeckli-Evans and H. U. Güdel, *Angew. Chem., Int. Ed.*, 2003, **42**, 4653.

12 V. K. Yachandra, K. Sauer and M. P. Klein, *Chem. Rev.*, 1996, **96**, 2927.

13 E. Adman, L. C. Sieker and L. H. Jensen, *American Crystallographic Association, Winter Meeting, Symposia: Experimental and theoretical studies of the electron density in crystals and molecules*, University of New Mexico, Albuquerque, N.M., 1972, Abstract L2.

14 P. Giastas, N. Pinotsis, G. Efthymiou, M. Wilmanns, P. Kyritsis, J.-M. Moulis and I. M. Mavridis, *J. Biol. Inorg. Chem.*, 2006, **11**, 445.

15 K. N. Ferreira, T. M. Iverson, K. Maghlaoui, J. Barber and S. Iwata, *Science*, 2004, **303**, 1831.

16 B. Schmid, H.-J. Chiu, V. Ramakrishnan, J. B. Howard and D. C. Rees, in *Handbook of Metalloproteins*, ed. A. Messerschmidt, R. Huber, T. Poulos and K. Wieghardt, Chichester, New York, Weinheim, Brisbane, Singapore, Toronto, 2001, p. 1025.

17 For example, see: (*a*) R. H. Holm, *Adv. Inorg. Chem.*, 1992, **38**, 1; (*b*) W. Lo, T. A. Scott, P. Zhang, C.-C. Ling and R. H. Holm, *J. Inorg. Biochem.*, 2011, **105**, 497; (*c*) A.-A. H. Abu-Nawwas, C. A. Muryn and M. A. Malik, *Inorg. Chem. Commun.*, 2009, **12**, 125.

18 For example, see: (*a*) C. C. Stoumpos, I. A. Gass, C. J. Milios, E. Kefalloniti, C. P. Raptopoulou, A. Terzis, N. Lalioti, E. K. Brechin and S. P. Perlepes, *Inorg. Chem. Commun.*, 2008, **11**, 196; (*b*) C. C. Stoumpos, N. Lalioti, I. A. Gass, K. Gkotsis, A. A. Kitos, H. Sartzi, C. J. Milios, C. P. Raptopoulou, A. Terzis, E. K. Brechin and S. P. Perlepes, *Polyhedron*, 2009, **28**, 2017.

19 For example, see: (*a*) H. Zhu, Q. Liu, C. Chen and D. Wu, *Inorg. Chim. Acta*, 2000, **306**, 131; (*b*) J.-L. Zuo, H.-C. Zhou and R. H. Holm, *Inorg. Chem.*, 2003, **42**, 4624; (*c*) A. Butler and C. J. Carrano, *Coord. Chem. Rev.*, 1991, **109**, 61.

20 G. S. Papaefstathiou, A. Escuer, M. Font-Bardía, S. P. Perlepes, X. Solans and R. Vicente, *Polyhedron*, 2002, **21**, 2027.

21 K. E. Gubina, V. A. Ovchynnikov, J. Swiatek-Kozlowska, V. M. Amirkhanov, T. Y. Sliva and K. V. Domasevitch, *Polyhedron*, 2002, **21**, 963.

22 S.-Y. Zhang, B. Xu, L. Zheng, W. Chen, Y. Li and W. Li, *Inorg. Chim. Acta*, 2011, **367**, 44.

23 J. A. Bertrand, E. Fijita and D. G. Vanderveer, *Inorg. Chem.*, 1979, **18**, 230.

24 M. Mikuriya, N. Nagao and K. Kondo, *Chem. Lett.*, 2000, 516.

25 S. Banerjee, M. Nandy, S. Sen, S. Mandal, G. M. Rosair, A. M. Z. Slawin, C. J. Gómez García, J. M. Clemente-Juan, E. Zangrando, N. Guidoling and S. Mitra, *Dalton Trans.*, 2011, **40**, 1652.

26 C.-M. Liu, Y. Song and D.-Q. Zhang, *Inorg. Chem. Commun.*, 2010, **13**, 160.

27 S. S. Tandon, S. D. Bunge, R. Rakosi, Z. Q. Xu and L. K. Thompson, *Dalton Trans.*, 2009, 6536.

28 J. A. Bertrand and T. C. Hightower, *Inorg. Chem.*, 1973, **12**, 206.

29 C. Dendrinou-Samara, C. A. Muryn, F. Tuna and R. E. P. Winpenny, *Eur. J. Inorg. Chem.*, 2010, 3097.

30 S. K. Langley, B. Moubaraki, C. M. Forsyth, I. A. Gass and K. S. Murray, *Dalton Trans.*, 2010, **39**, 1705.

31 S. J. Shah, C. M. Ramsey, K. J. Heroux, J. R. O'Brien, A. G. DiPasquale, A. L. Rheingold, E. Del Barco and D. N. Hendrickson, *Inorg. Chem.*, 2008, **47**, 6245.

32 V. Tangoulis, M. Skarlis, C. P. Raptopoulou and C. Dendrinou-Samara, submitted.

33 C.-M. Liu, Y. Song and D.-Q. Zhang, *Inorg. Chem. Commun.*, 2010, **13**, 160.

34 M. Murugesu, W. Wernsdorfer, K. A. Abboud and G. Christou, *Angew. Chem., Int. Ed.*, 2005, **44**, 892.

35 C. P. Pradeep, P. S. Zacharias and S. K. Das, *Eur. J. Inorg. Chem.*, 2007, **34**, 5377.
36 (*a*) Z.-G. Li, J.-W. Xu, H.-Q. Jia and N.-H. Hu, *Inorg. Chem. Commun.*, 2006, **9**, 969; (*b*) Z. Boulsourani, V. Tangoulis, C. P. Raptopoulou, V. Psycharis and C. Dendrinou-Samara, *Dalton Trans.*, 2011, **40**, 7946.
37 (*a*) M. Gatehouse, S. E. Livingstone and R. S. Nyholm, *J. Inorg. Nucl. Chem.*, 1958, **8**, 75; (*b*) N. T. Madhu and P. K. Radhakrishnan, *Transition Met. Chem.*, 2000, **25**, 287; (*c*) K. Nakamoto, *Infrared and Raman Spectra of Inorganic and Coordination Compounds*, Wiley, New York, 1986; (*d*) K.-E. Lee and S. W. Lee, *J. Mol. Struct.*, 2010, **975**, 247.
38 O. Roubeau and R. Clérac, *Eur. J. Inorg. Chem.*, 2008, 4325.
39 R. A. Coxall, S. G. Harris, D. K. Henderson, S. Parsons, P. A. Tasker and R. E. P. Winpenny, *J. Chem. Soc., Dalton Trans.*, 2000, 2349.
40 (*a*) I. D. Brown and K. W. Wu, *Acta Crystallogr., Sect. B: Struct. Crystallogr. Cryst. Chem.*, 1976, **32**, 1957; (*b*) H. H. Thorp, *Inorg. Chem.*, 1992, **31**, 1585.
41 The diagonalization of the energy matrix has been done numerically using the MAGPACK program. J. J. Borras-Almenar, J. M. Clemente-Juan, E. Coronado and B. S. Tsukerblat, *J. Comput. Chem.*, 2001, **22**, 985.
42 N. C. Pastor, J. B. Serra, E. Coronando, G. Pourroy and L. C. W. Baker, *J. Am. Chem. Soc.*, 1992, **114**, 10380.
43 C. J. G. Garcia, E. Coronando and J. B. Almenar, *Inorg. Chem.*, 1992, **31**, 1667.
44 R. Boca, *Coord. Chem. Rev.*, 2004, **248**, 757.
45 L. F. Chibotaru, J.-J. Girerd, G. Blondin, T. Glaser and K. Wieghardt, *J. Am. Chem. Soc.*, 2003, **125**, 12615.
46 A. Abragam and B. Bleaney, in *Electron Paramagnetic Resonance of Transition Ions*, Clarendon Press, Oxford, U.K., 1970.
47 M. Handa, N. Koga and S. Kida, *Bull. Chem. Soc. Jpn.*, 1988, **61**, 3853.
48 N. A. Law, J. W. Kampf and V. L. Pecoraro, *Inorg. Chim. Acta*, 2000, **297**, 252.
49 K. K. Nanda, L. K. Thompson, J. N. Bridson and K. Nag, *J. Chem. Soc., Chem. Commun.*, 1994, 1337.
50 *Rigaku/MSC CrystalClear*, Rigaku/MSC Inc., The Woodlands, Texas, USA, 2005.
51 G. M. Sheldrick, *SHELXS-97: Structure Solving Program*, University of Göttingen, Göttingen, Germany, 1997.
52 G. M. Sheldrick, *SHELXL-97: Crystal Structure Refinement Program*, University of Göttingen, Göttingen, Germany, 1993–7.